SciMedCentral

JSM Sexual Medicine

Research Article

# Utilizing Folate-Gold Nanorods Mediated Photothermal Ablation to Eliminating Cancer Cells from Spermatogonial Stem Cells *In vitro*

**Neda Eslahi[1,2], Tahereh Tohidi-Moghadam[3], Vahid Pirhajati-Mahabadi[4], Amirhossein Mohammadi[2,5], Azar Shams[6], Hamidreza Asgari[2,5], Seyed Mohsen Razavi[7], Seyed Rouhallah Miri[8] and Morteza Koruji[2,5]***

[1]*Finetech in Medicine Research Center, Iran University of Medical Sciences, Iran*

[2]*Stem Cell and Regenerative Medicine Research Center, Iran University of Medical Sciences, Iran*

[3]*Department of Nanobiotechnology, Tarbiat Modares University, Iran*

[4]*Neuroscience Research Center, Iran University of Medical Sciences, Iran*

[5]*Department of Anatomy, School of Medicine, Iran University of Medical Sciences, Iran*

[6]*Department of Reproductive Biology, Pishgam Payazist Research and Knowledge Based Company, Iran*

[7]*Clinic of Hematology and Oncology, Firozgar Hospital, Iran University of Medical Sciences, Iran*

[8]*Department of Surgical Oncology, Cancer Institute, Tehran University of Medical Science, Iran*

***Corresponding author**

Morteza Koruji, Stem Cell and Regenerative Medicine Research Center & Department of Anatomy, School of Medicine, Iran University of Medical Sciences (IUMS), Hemmat Highway, P. O. Box 14155-5983, Tehran, Iran, Tel: +98 21 88622689

**Submitted:** 19 April 2025
**Accepted:** 29 July 2025
**Published:** 31 July 2025

**ISSN:** 2578-3718



**Keywords**

- Spermatogonial stem cells
- Gold nanorods
- EL4 cells
- Folic acid
- Cytotoxicity
- Laser therapy

## Abstract

Cancer therapies such as chemotherapy and radiation are known to jeopardize fertility, potentially causing sperm DNA damage and leading to temporary or permanent infertility. Despite the benefits of these treatments in combating cancer, the risk of contamination of spermatogonial stem cells (SSCs) by residual cancer cells remains a significant concern in fertility preservation. This study aimed to address this issue by evaluating the efficacy of a novel approach involving the use of folate-conjugated silica-gold nanorods (F-Si-GNRs) in conjunction with laser therapy to eliminate EL4 malignant cells from spermatogonial stem cells. The experimental procedure involved subjecting spermatogonial stem cells and EL4 cells to an 808 nm, 2.5 W laser after pre-incubation with 100 μM F-Si-GNRs. Following treatment, the cellular composite was transplanted into recipient mice to assess tumorigenicity. Toxicity levels were evaluated using MTT assays, while apoptosis rates were determined through flow cytometry analysis. Results revealed survival rates of 45.33 ± 0.8% for SSCs and 6.6 ± 0.08% for EL4 cells post-treatment. Encouragingly, no signs of tumorigenicity were detected in mice receiving the transplanted cells. This innovative combination of F-Si-GNRs and laser therapy holds promise as an effective strategy for removing tumorigenic cells from SSCs prior to transplantation. By mitigating the risk of cancer cell contamination, this approach offers a potential avenue for enhancing the success of fertility preservation procedures in cancer patients undergoing treatment.

## INTRODUCTION

Cancer treatment modalities such as chemotherapy and radiation therapy, while effective in combating malignancies, often exact a toll on patients' reproductive capacity, leading to complications such as sperm DNA damage and potential infertility, whether temporary or permanent [1]. Notably, there has been a marked improvement in the survival rates of pediatric cancer patients in recent years, with approximately 1 in 530 individuals with cancer responding favorably to therapy. Among childhood cancers, Acute Lymphoblastic Leukemia (ALL) holds prominence, constituting 34% of all cancer diagnoses among children under 14 [2]. Despite advancements in treatment outcomes, fertility preservation remains a paramount concern for survivors, particularly in light of the lingering effects of infertility and hypogonadism following therapy. For children who have undergone successful treatment, the prospect of infertility looms large, necessitating proactive measures. Testicular biopsy emerges as a viable option, particularly for prepubescent individuals, with the aim of isolating Spermatogonial Cells (SCs) for potential transplantation post-puberty. However, this approach underscores the urgent need for innovative strategies to safeguard and restore fertility in cancer survivors, given the inherent

limitations and uncertainties associated with current methods.

However, there exists a considerable risk of contamination of SCs by residual cancer cells. Exposure to chemotherapy drugs can disrupt the hypothalamic-pituitary-gonadal axis in men, impacting testicular function. The testes play dual crucial roles: they are responsible for sperm production through germ cell differentiation within the seminiferous tube epithelium, and they produce testosterone, vital for the development and maintenance of secondary sexual characteristics in men and the sustenance of spermatogenesis during puberty [2]. Studies have indicated that germ cell transplantation from leukemic mice resulted in tumor growth, underscoring the necessity of complete segregation of tumor cells from germ cells [3]. Presently, techniques such as Magnetic-Activated Cell Sorting (MACS) and Fluorescence-Activated Cell Sorting (FACS) are employed to isolate spermatogonial cells from heterogeneous cell populations obtained from biopsied samples in both murine and human testicular cell suspensions. However, challenges persist in achieving purification based on these methods due to variations in cell size and the expression of surface antigens on leukemic testicular cells.

Furthermore, the efficacy of MACS in preventing leukemia recurrence in PVG rats when using cells from leukemic testes for testicular cell transplantation is limited [4]. These findings underscore the need for novel approaches to ensure the complete elimination of tumor cells from germ cell populations, emphasizing the urgency for further research and innovation in this field.

In an previous phase of our investigation, we explored the efficacy of Folate-Silica-Gold Nanorods (F-Si-GNRs) in targeting both mouse acute lymphoblastic leukemia (EL4 cancerous cell line) and spermatogonial cells to eradicate cancerous cells [5]. Gold Nanorods, a component of this novel approach, possess the unique ability to absorb both UV and infrared radiation, thereby generating heat, which plays a pivotal role in the destruction of cancer cells [6]. This mechanism aligns with previous pioneering work by Hirsch et al., who demonstrated the groundbreaking use of gold nanoparticles combined with laser therapy in targeting epithelial cells in human SKBr3 breast cancer [7]. Such interdisciplinary endeavors highlight the potential of nanotechnology-assisted therapies in revolutionizing cancer treatment paradigms.

Numerous experiments have delved into the intricate interplay between laser parameters and cellular responses, recognizing the pivotal role of nanoparticle properties such as size and shape in modulating cellular penetration. The initiation of cell damage, characterized by phenomena like microbubble formation, membrane blebbing, and apoptosis, arises from the targeted binding of nanoparticles and localized energy delivery. This precision targeting holds promise in minimizing collateral damage to healthy cells and tissues [8]. For instance, Zharov et al., scrutinized bubble formation induced by nanoparticles measuring 40 nm in diameter, noting cell death and cluster formations following exposure to either 30 pulses of 0.5 J/cm2 or a single pulse of 2 J/cm2 [9]. Similarly, Huang et al., explored cancer cell apoptosis across varying energy efficacies, elucidating pathways wherein high laser strength results in nanoparticle fragmentation inducing an electric shock to cells, while lower laser strength generates heat from nanoparticles, ultimately perforating cell membranes and leading to cell demise [10].

In light of the advantageous impact of laser therapy on tumor cells, we embarked on an extensive research endeavor to investigate the synergistic effects of utilizing F-Si-GNRs in tandem with laser therapy for purifying SCs from EL4 cells. The initial phase of our study entailed the investigation of gold nanoparticles coated with silica and conjugated with folic acid, wherein varying doses of nanoparticles were administered separately to SCs and EL4 cells to ascertain the optimal threshold for apoptosis induction [5]. Building upon this foundation, the subsequent phase integrated laser technology into the synthesized nano-system, enabling an exploration of the combined effect of laser irradiation and gold nanorods on the cellular mixture of SCs and EL4 cells. This comprehensive approach aims to advance our understanding of novel therapeutic strategies for purifying stem cells and holds immense potential for enhancing cancer treatment outcomes.

## METHODS AND MATERIALS

We utilized 120 neonatal NMRI mice aged between 3 to 6 days, sourced from the Experimental and Comparative Studies Center at Iran University of Medical Sciences (IUMS). These animals were housed in cages maintained at a temperature range of 22-25 °C, under a 12-hour light-dark cycle, with ad libitum access to food and water. All experimental procedures adhered to ethical standards established by the Animal Care and Use Committee (ACUC) at Iran University of Medical Sciences, as per registration code 94-01-117-25884. EL4 cancer cells were selected for this study due to their resemblance to human lymphoblastic cancer cells. Originating from a C57BL mouse-induced lymphoma, EL4 cells represent a T lymphoblast line. Chemicals utilized in the study, including HAuCl4·3H2O (Tetrachloroauric (III) acid trihydrate),

NaBH4 (Sodium borohydride), Ascorbic acid, CTAB (Hexadecyl trimethyl ammonium bromide), AgNO3 (Silver nitrate), TEOS (Tetraethylorthosilicate), and Folate, were procured from Sigma (Germany). Additionally, Phosphate Buffered Saline (PBS) tablets and Sodium acetate were sourced from Merck (USA).

### Isolation and validation of SCs and EL4 cells

SCs were isolated using a two-step enzymatic digestion process. To enhance purification, they were subsequently cultured in 3 cm dishes for 24 hours, allowing Sertoli and myoid cells to adhere to the bottom of the culture dishes. The remaining non-adherent cells were gently removed from the solution. Following this, the cells were cultured again in Dulbecco's Modified Eagle Medium (DMEM) supplemented with 5% serum, 1.37 g/L NaHCO3, penicillin (100 IU/mL), streptomycin (100 µg/mL), and nonessential amino acids. The EL4 cell line was sourced from the Pasteur Institute and cultured using DMEM/F12 medium containing 1% Fetal Bovine Serum (FBS). Flow cytometry was employed to confirm the identity of both SCs and EL4 cells. For SCs, the expression of Plzf was assessed using a PLZF monoclonal antibody, while EL4 cells were confirmed using a FITC-conjugated mouse anti-H-2kb monoclonal antibody. Furthermore, the expression of specific spermatogonial cell genes including Oct-4, Gfra, Plzf, VASA, Igα6, and Igβ1 was examined via RT-PCR. To validate the identity and functionality of both cell types, transplantation experiments were conducted using an azoospermia mouse model. These comprehensive methodologies ensure the accurate characterization and utilization of SCs and EL4 cells for further experimental investigations [5].

### Co-culture of SCs and EL4 cells

SCs were co-cultured with EL4 cells at a 5% contamination rate (95% SCs & 5% EL4 cells) and incubated in DMEM/F12 medium (Gibco) supplemented with 2% fetal bovine serum, penicillin (100 U/mL), streptomycin (100 µg/mL), and gentamycin (40 µg/mL). The cell population was subsequently divided into five experimental groups: Group 1 served as the control, receiving only the medium; Group 2 was treated with 100M Si-GNRs in the medium; Group 3 received 100M F-Si-GNRs, a dose determined during the preliminary phase of experimentation; Group 4 underwent laser irradiation alone; and Group 5 was exposed to both 100M F-Si-GNRs and laser irradiation. Flow cytometry was utilized to evaluate the expression of specific markers for each cell type (Plzf for SCs and H-2Kb for EL4 cells), enabling a comprehensive assessment of the effects of various treatments on cellular behavior and phenotype.

### Synthesis of F-Si-GNRs combined with Near-infrared (NIR) laser

Gold nanorods with dimensions of 20.44 ± 1.8 nm in length and 5.55 ± 1.56 nm in width were synthesized using the sequential seed interference growth process (11). Following synthesis, their surfaces underwent modification with silica and folate. The cells were subjected to laser irradiation using an 808 nm, 2.5 W laser (Nanobon Corporation, Tehran, Iran). The synthesis process began with the mixing of aqueous solutions of HAuCl4 ·3H2O (250 µL, 0.01 M) and CTAB (7.5 mL, 0.095 M), followed by the rapid addition of an ice-cold NaBH4 (600 µL, 0.01M) solution, leading to the formation of a growth solution. Subsequently, CTAB (9.5 mL, 0.095 M), HAuCl4 ·3H2O (400 µL, 0.01 M), AgNO3 (60 µL, 0.01 M), and ascorbic acid (64 µL, 0.10 M) solutions were sequentially added to the mixture to induce the formation of small spherical nanoparticles. Further rod formation was facilitated by centrifugation of the solution and removal of excess CTAB. In the final step, the gold nanorods' surfaces were coated with silica by sequentially adding 20 µl of TEOS (diluted to 1 mL with ethanol) to the GNRs (20 µL each time) at 30-minute intervals, followed by overnight purification to obtain silica-coated GNRs (Si-GNRs). For targeted surface coating of the nanorods, folate was selected due to the overexpression of the folate receptor (FR) on many tumor cells, making it a recognized biomarker for cancer. To conjugate nanoparticles with folate, 1.5 mg of folate was dissolved in 2 ml of dimethyl sulfoxide (DMSO), and for every 10 ml of GNR suspension in ethanol, 250 µl of folate solution was used. FTIR spectrum analysis was employed to confirm silica-coated GNRs before and after folic acid binding. For morphology confirmation and size evaluation, the nanoparticles were placed on a copper grid covered with carbon, dried under ambient conditions, and imaged using a transmission electron microscope (TEM) from Zeiss (LEO 906, 100KV). Additionally, electron microscopy was utilized to trace rod-shaped nanoparticles within cells, providing insights into their intracellular localization and distribution.

### Cytotoxicity of F-Si-GNRs combined with NIR laser light on SCs and EL4 cells

Cells were seeded into a 96-well plate at a density of 15×103 cells per well. Following seeding, the cells were incubated with 100 M F-Si-GNRs for a duration of 6 hours before being subjected to laser irradiation for varying exposure periods (5, 10, 20, 30 minutes). The viability of the cells post-irradiation was assessed using the MTT assay. To evaluate potential toxicity, the cells were centrifuged and washed with PBS prior to conducting

the MTT assay. Subsequently, 100 µl of MTT solution (5 mg/ml MTT tetrazolium salt) was added to each well and incubated for 3–4 hours. Following incubation, the solution was centrifuged, and the supernatant was removed. Next, 100 µl of DMSO was added to each well, and the plates were subjected to agitation for 10 minutes using an ELISA reader set to 570 nm for colorimetric measurement. Despite the inherent differences in the nature of cells in the plate (one adherent and one suspended), the uniformity of the 6-hour incubation period allowed for consistency in the exposure of both cell types to F-Si-GNRs combined with NIR irradiation. This standardized approach facilitated comparative analysis of cellular responses, notwithstanding variations in cell adhesion kinetics.

### Apoptosis in SCs and EL4 cells following treatment with F-Si-GNRs and NIR laser

Flow cytometry served as the pivotal tool for identifying apoptosis utilizing the annexin V–fluorescein isothiocyanate (FITC)/propidium iodide (PI) apoptosis detection kit. Initially, cells were seeded into 24-well plates at a density of 200,000 cells per well. Following a thorough washing with PBS and subsequent re-suspension in annexin binding buffer, cells were incubated in the dark for 15 minutes with annexin V–FITC/PI. Subsequently, the number of viable, early apoptotic, late apoptotic, and necrotic cells was quantified using a flow cytometer. Early apoptotic cells were characterized by their positive staining for annexin-V–FITC but negative staining for PI, whereas late apoptotic cells exhibited positive staining for both annexin-V–FITC and PI. Necrotic cells, on the other hand, displayed positive staining for PI but negative staining for annexin-V–FITC. This comprehensive analysis enabled the precise delineation of apoptotic cell populations, shedding light on the intricate dynamics of cellular responses to experimental conditions.

### Tumorigenicity of EL4 cells in co-culture following treatment

To ensure the precision and reliability of histological examination post-transplantation, it was imperative that the mice were rendered azoospermic prior to transplantation, ensuring the seminiferous tubules were devoid of contents. Consequently, azoospermia was induced in mice using busulfan before the transplantation procedure. Following treatment, the cells were transplanted into the efferent ductules of azoospermic NMRI mice, which were male, aged 6–8 weeks, and weighed between 20–30 g. Two months post-transplantation, the abdominal region of the mice was meticulously examined for the presence of any tumors, and subsequently, their testicles were dissected and prepared for histological examination. This stringent protocol ensured thorough evaluation of both the transplanted cells and any potential tumorigenicity, providing crucial insights into the efficacy and safety of the transplantation procedure.

### Statistical analysis

The data are depicted as the mean ± Standard Deviation (SD) of a minimum of three biologically independent replicates. Group distinctions were evaluated utilizing two-way analysis of variance (ANOVA) performed with SPSS version 26. Apoptosis rates were further scrutinized through ANOVA followed by Tukey's post-hoc test for multiple comparisons. A significance level was established at $p \leq 0.05$ to ascertain statistically significant differences between experimental groups.

## RESULTS

### Confirmation of cells

Flow cytometry analysis revealed that the average expression of PLZF in SCs was 45.6 ± 5.7% at the conclusion of the first week of culture, escalating to 84.7 ± 4.02% by the end of the second week. Additionally, the expression of specific markers associated with SCs, including 4 Oct- GFRa, PLZF, VASA, Igα6, Igβ1, along with GAPDH as a housekeeping gene, was assessed. To probe the functionality of SCs, these cells were transplanted into the testes of azoospermic mice after being labeled with DiI and DAPI. Direct injection of 105 cells into the efferent ducts of azoospermic mice facilitated transplantation. After an 8-week period post-transplantation, tissue sections were meticulously prepared and examined under a fluorescent microscope. Confirmation of EL-4 cells was achieved through H-2Kb monoclonal antibody staining, revealing a specific expression of the H-2Kb marker on the surface of tumor cells, with an average expression of 96.25 ± 2.81%. Subsequently, to validate the tumorigenic potential of EL-4 cells, these cells were transplanted into the efferent ducts of the testes in azoospermic mice. Four weeks post-transplantation, the morphology and dimensions of the testicular tissue were evaluated. Histological analyses unveiled tumor formation in 70% of the mouse testicular tissue after 4 weeks, with an average tumor size measuring 142 mm (Figure 1).

### Assessments of F-Si-GNRs

The FTIR spectrum analysis depicted in Figure 2C showcases the transformation in spectral characteristics upon modifying silica-coated Gold Nanorods (GNRs) with folic acid. The incorporation of folic acid, consisting of

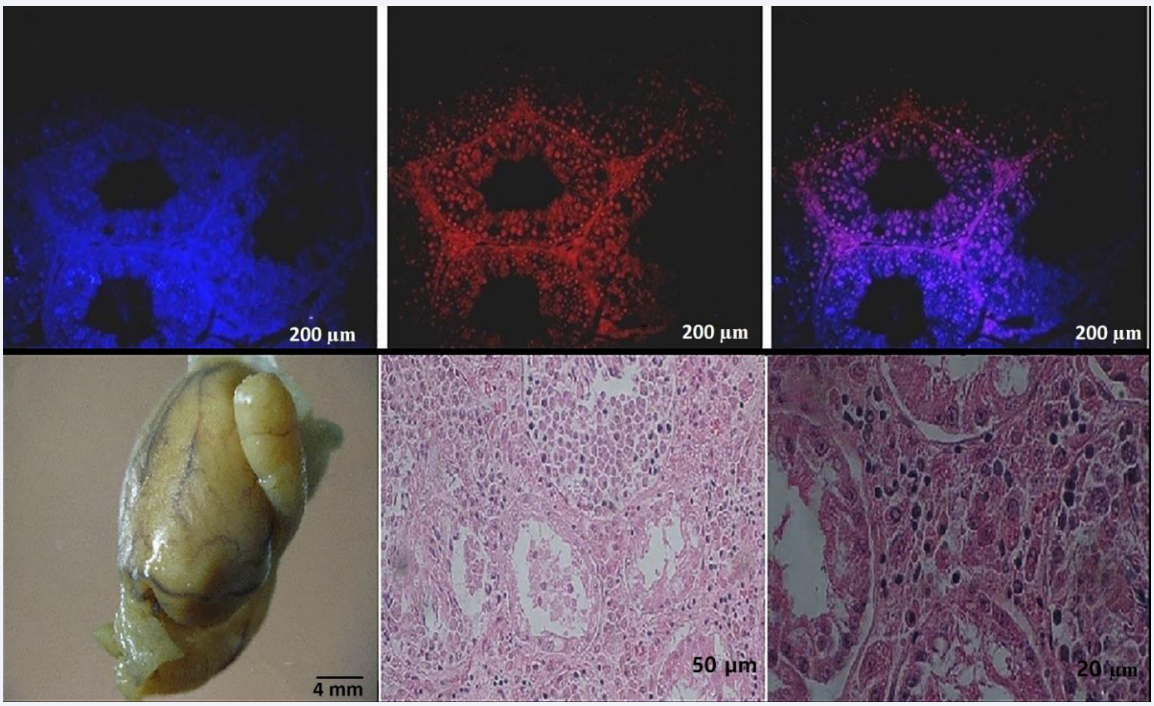


**Figure 1** Visualization of Cell Labeling and Tumor Formation in Transplanted Mice Testes. A: SCs were labeled with DAPI to visualize their nuclei. B: DiI-labeled SCs were observed under fluorescence microscopy, indicating successful labeling. C: The merged image shows the localization of DiI-labeled SCs within the testicular tissue (scale bar: 200 µm). D: Tumor tissue formed after transplantation of EL4 cells into the efferent duct of azoospermia mice. The average tumor size was 142 mm, highlighting successful tumor establishment (scale bar: 4 mm). E, F: Cross-sections reveal structural alterations in the seminiferous tubules and infiltration of leukemic cells post-tumor cell transplantation. E (scale bar: 50 µm) and F (scale bar: 20 µm) depict the extent of tissue disruption and leukemic cell infiltration, emphasizing the invasive nature of the tumor cells.

p-aminobenzoic acid, glutamic acid, and heterobicyclic pteridine, led to discernible changes in vibrational bands. Notably, specific vibrational bands corresponding to the phenyl and pterin ring (PT) (around 11478 cm-1), as well as the OH of carboxylic acid of glutamic acid and NH group of pterin ring stretching within the range of 3500-3700 cm-1, underscored the absorption of folic acid molecules onto the gold nanorod matrix. Further elucidation of the morphology and dimensions of gold nanorods with silica coating (Figure 2A, B), was accomplished using electron microscopy. The histogram representing the size distribution of gold nanorods revealed a length of 20.43 ± 2.18 nm and a width of 5.55 ± 1.56 nm (Figure 2C). Noteworthy changes in the Surface Plasmon Resonance (SPR) bands were observed subsequent to the formation of a silica layer around the nanostructure. Upon the addition of Tetraethylorthosilicate (TEOS), a decline in the intensity of the absorption band of the longitudinal surface plasma signified the formation of a silica layer around the nanostructures, while the transversal surface plasmon absorption group exhibited minimal alteration. The coating of GNRs with a very thin silica layer (2.56 ± 0.62 nm) not only augmented the colloidal stability of the nanorods but also stabilized their shape while modifying their surface properties. Furthermore, Zeta potential analysis indicated a notable shift in surface charge from +37 before the addition of folic acid to -10 after conjugation with folic acid, corroborating the presence of folic acid on the nanoparticle surface. Zeta potential measurements served as an integral tool for determining the surface charge of the nanoparticles, thus providing valuable insights into their surface characteristics and functionalization.

## Evaluation of the viability of both cell types after laser irradiation

Following the laser exposure experiments, the assessment of cell viability was conducted. Surprisingly, the survival rate exhibited negligible variance across different durations of laser exposure. Consequently, a 5-minute incubation period emerged as the optimal choice (Figure 3A). Subsequently, cells were subjected to a 6-hour incubation with 100 M F-Si-GNRs prior to a 5-minute laser irradiation, and their viability was evaluated using the MTT assay. The results unveiled a slight reduction in

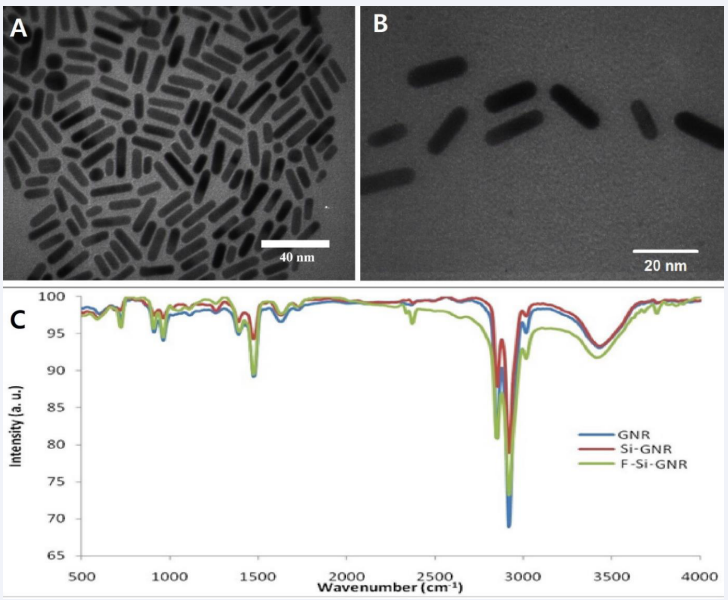


**Figure 2 Transmission Electron Microscopy and Spectral Analysis of Gold Nanorods.** A, B: Transmission electron microscopy images depict gold nanorods coated with silica. The thickness of the silica layer was measured to be 2.56 ± 0.62 nm. A (scale bar: 40 nm) and B (scale bar: 20 nm) provide detailed views of the nanorod morphology. C: Spectral analysis illustrates the characteristic surface plasmon resonance (SPR) bands of gold nanorods before and after surface modification with silica and folate. The spectra compare silica-coated gold nanorods (Si-GNR) with folic acid-modified silica-coated gold nanorods (F-Si-GNR).

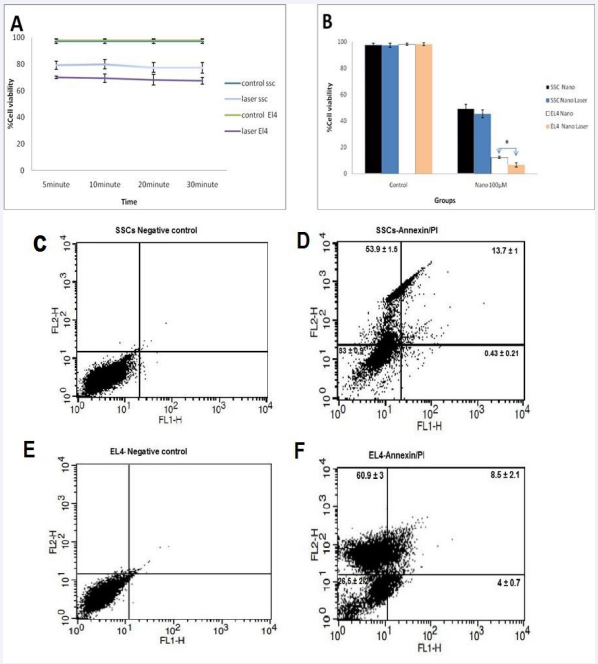


**Figure 3 Assessment of Laser Irradiation and Gold Nanoparticle Dose.** A: The graph illustrates the impact of varying laser irradiation durations on cell viability. B: MTT assay results depict the viability of EL4 tumor cells and SCs after 6 hours of incubation with different doses of gold nanoparticles followed by 5 minutes of laser irradiation. C, D: Flow cytometry data show the effects of laser therapy on SSCs, revealing changes in apoptosis and necrosis rates. E, F: Flow cytometry analysis demonstrates alterations in apoptosis and necrosis rates in EL4 tumor cells following laser therapy.

*: Denotes significant differences in the survival rate of EL4 tumor cells before and after laser irradiation ($p \leq 0.05$).

the viability of SCs from 49 ± 3% to 45.33 ± 2.8% post-laser therapy, which, albeit a decrease, did not manifest as a significant decline. Conversely, a notable decline in viability was observed in EL4 cells, plummeting from 12.3 ± 2.51% to 6.6 ± 0.8% post-laser therapy (Figure 3B). This significant reduction in viability underscores the efficacy of laser therapy in targeting and impairing the viability of these malignant cells, highlighting its potential as a therapeutic intervention in cancer treatment.

### Assessment of apoptosis and ultrastructure of SCs and EL4 cells

The Annexin kit served as a crucial tool for assessing cell apoptosis/necrosis subsequent to the incubation of SCs and EL4 cells with 100 M F-Si-GNRs for 6 hours followed by a 5-minute laser application. Flow cytometry analysis revealed necrosis frequencies of 53.9 ± 1.5% for SCs and 60.9 ± 3% for EL4 cells (Figure 3B). Notably, the survival rates for SCs and EL4 cells post-treatment were 32.9 ± 0.8% and 26.5 ± 2.2% respectively, exhibiting a significant decrease compared to pre-laser therapy rates of 66.7 ± 2% and 46.7 ± 5.8% respectively. Similarly, apoptosis rates for SCs and EL4 cells post-treatment were 12.5 ± 2.6% and 14.1 ± 1.1% respectively, representing a remarkable reduction from pre-treatment rates of 32.9 ± 2% and 51.1 ± 6% respectively (Figure 3C-F). Prior to laser therapy, no necrotic SCs or EL4 cells were detected, highlighting a significant change in the necrosis rate post-laser therapy. Notably, the combination of F-Si-GNRs and laser treatment induced both apoptosis and necrosis in the cells, with necrosis being more prevalent than apoptosis (Figure 4A-C). Ultrastructural examination of EL4 cells post-laser treatment revealed aberrations such as an atypical nucleus, complete disruption of the cell membrane, mitochondria, and crystals, along with empty organelle bubbles protruding from the plasma membrane, indicative of necrosis (Figure 5A-F). Conversely, in SCs, distinct markers of apoptosis including chromatin condensation, plasma membrane bubbles containing cellular organelles, mitochondrial disruption, and phagocytic vacuoles were observed, underscoring the apoptotic pathway (Figure 5A-F). Notably, electron microscopic images post-laser irradiation revealed pronounced necrosis characterized by general cell swelling and accelerated loss of plasma membrane integrity compared to pre-treatment images. These comprehensive findings shed light on the intricate mechanisms underlying cell fate modulation in response to F-Si-GNRs and laser therapy, emphasizing the dual induction of apoptosis and necrosis as potential avenues for cancer treatment.

### Flow cytometry analysis of SCs and EL4 cells

After treatment, the composition of the two cell groups in co-culture was assessed via flow cytometry analysis (Figure 6). Notably, the proportion of cells expressing PLZF and H-2Kb markers varied across the treatment groups. In the Si-GNRs group, the proportion was 82.1 ± 3.8% and 4.6 ± 1%, respectively, while in the F-Si-GNRs group, it was 62.8 ± 3.6% and 1.9 ± 0.27%, in the laser treatment group, it was 61.3 ± 6.7% and 2.1 ± 0.38%, and in the F-Si-GNRs combined with laser therapy group, it was 30.6 ± 7.7% and 0.53 ± 0%, respectively. Notably, the survival rate of SCs in the F-Si-GNRs and laser therapy group was significantly higher compared to other groups. Similarly, with EL4 cells, the group subjected to F-Si-GNRs and laser therapy exhibited significant differences from the Si-GNRs treated or control groups. However, no significant variance was observed between the laser-treated and F-Si-GNRs groups (Figure 6).

Furthermore, we investigated alterations in surrounding temperature in laser-treated and nano-treated groups employing laser therapy on SCs, EL4 cells, and co-culture medium. As depicted in Figure 6, the temperature of laser-irradiated cells increased to 34.2°C in the normal cell group, and following 6 hours of NP incubation and laser application, it rose to 39.5°C. Conversely, in the cancer cell group, the temperature of laser-irradiated cells reached 40.1°C, escalating to 56.2°C after 6 hours of NP incubation and laser exposure. In the group co-culturing healthy and cancer cells, the temperature of laser-irradiated cells was 36.6°C, elevating to 43.4°C after 6 hours of NP incubation and laser application. Remarkably, the temperature in the cancer cell group after NP incubation and laser exposure surpassed the hyperthermia threshold, reaching 56.2°C. Considering the hyperthermia temperature range between 41 and 45 degrees, this temperature elevation could lead to tissue damage and cell necrosis, highlighting the potential impact of hyperthermia induced by NP and laser treatment.

### Tumorigenicity of EL4 cells in co-culture following treatment

The testes of recipient mice were extracted, fixed, and sectioned eight weeks following the co-culture of cells subjected to F-Si-GNRs and laser therapy. In contrast to the control group where tumor cells were detectable in the interstitial spaces, no tumor cells were observed in the cross-sections of the experimental group (Figure 7C, D). This absence of tumor cells suggests the efficacy of the combined treatment in suppressing tumor formation, presenting a promising outcome for therapeutic intervention.

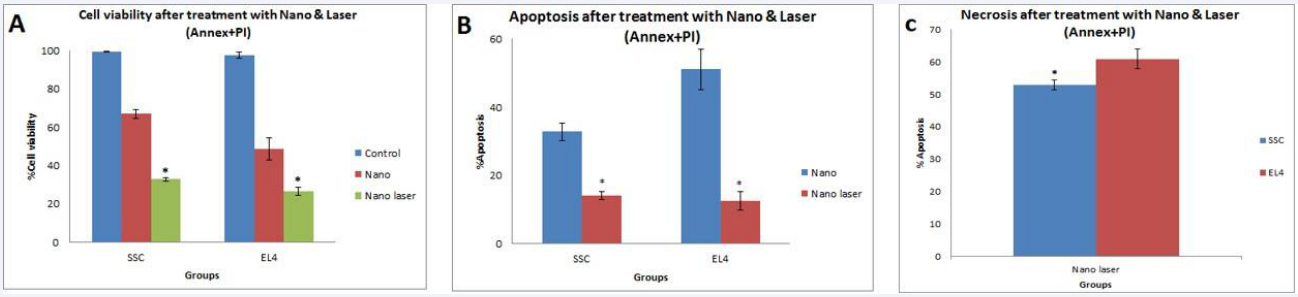


**Figure 4 Comparative Analysis of SCs and EL4 Cells**. A: The bar graph illustrates the survival rates of SCs and EL4 cells after incubation with gold nanoparticles and 5 minutes of laser irradiation. B: The graph shows the levels of apoptosis observed in SCs and EL4 cells following treatment with gold nanoparticles and laser irradiation. C: The bar graph depicts the extent of cell necrosis in SCs and EL4 cells after exposure to gold nanoparticles and laser irradiation for 5 minutes.

*: Indicates significant within-group differences in each experimental group ($p \leq 0.05$).

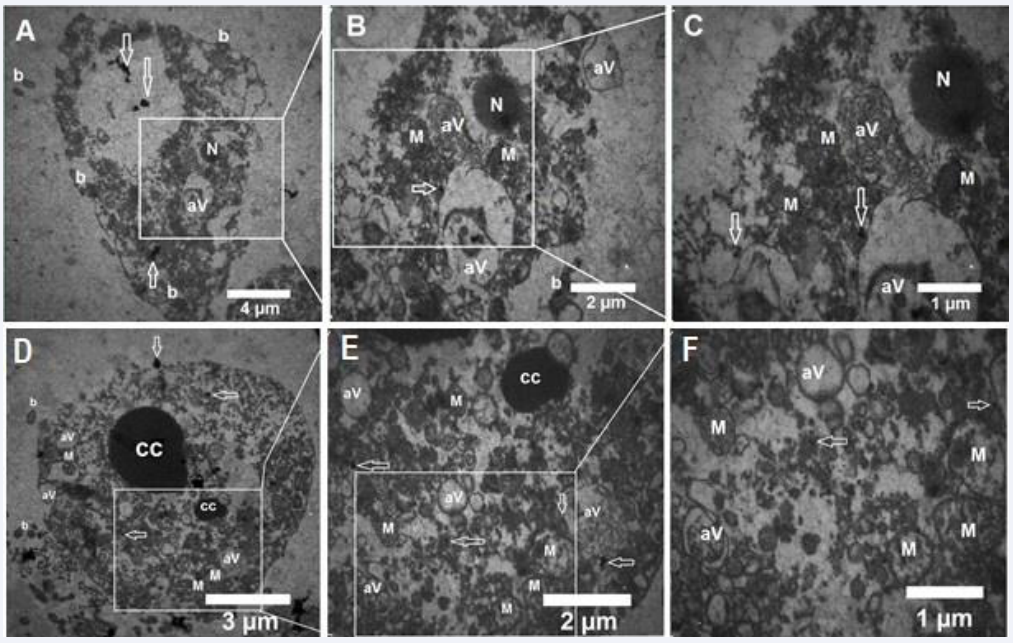


**Figure 5 Ultrastructural Analysis of EL4 and SCs.** A-C: Transmission electron microscopy images of EL4 cells post-incubation with gold nanoparticles and laser irradiation. These images reveal atypical nuclei, mitochondrial damage, phagocytic vacuoles, and plasma membrane-derived bubbles lacking organelles. D-F: Transmission electron microscopy images of SSCs after exposure to gold nanoparticles and laser irradiation. These images showcase chromatin cleavage and condensation, plasma membrane-derived bubbles containing cellular organelles, mitochondrial damage, and phagocytic vacuoles. M: Mitochondria, N: Nucleus, White Arrows: Gold Nanoparticles, aV: Phagocytic Vacuoles, b: Plasma Membrane Blebbing, CC: Condensed Chromatin.

## DISCUSSION

Childhood cancers pose challenges like sperm DNA damage and potential infertility in prepubertal patients despite chemotherapy and radiotherapy treatments [11]. While stem cell transplantation offers a potential solution for preserving fertility, the risk of residual tumor cell contamination inhibits its widespread use. Techniques like FACS and MACS have shown limited efficacy in eliminating these cells [12]. Various studies have attempted to overcome this challenge with varying success rates. For instance, Fujita et al. successfully removed SCs from leukemia cells using FACS, preventing leukemia recurrence post-transplantation [13]. Conversely, Geen

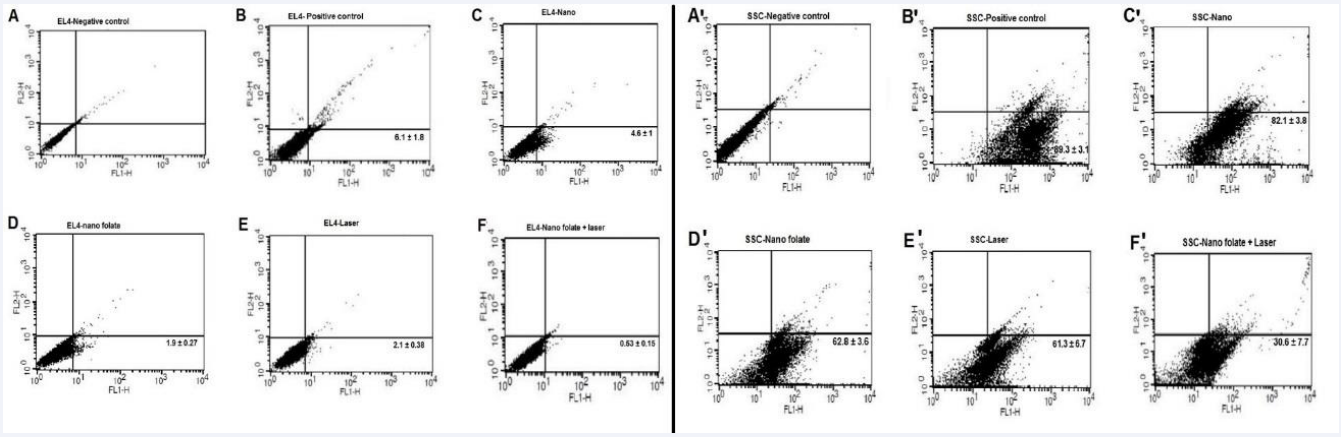


**Figure 6 Flow Cytometry Analysis of EL4 and SCs.** A-F: EL4 Cells, A′-F′: SCs, A, A′: Negative Control, B, B′: Positive Control, C, C′: Cells with Gold Nanoparticles, D, D′: Cells with Gold Nanoparticles Conjugated to Folate, E, E′: Cells with Laser Irradiation, F, F′: Cells with Gold Nanoparticles Conjugated to Folate and Laser Irradiation

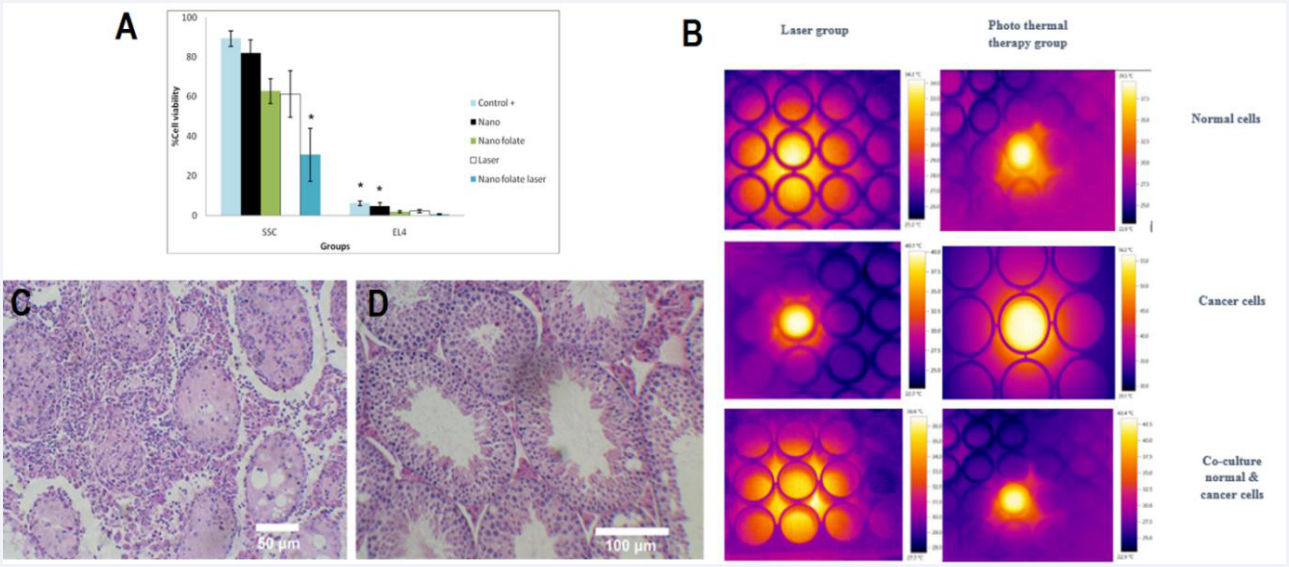


**Figure 7 Evaluation of Cell Viability and Temperature Profile.** A: Viability Assessment of SCs and EL4 Cells in Co-culture. B: Temperature Profile Increase in SCs, EL4, and Co-culture Groups. C: H&E-Stained Histological Assay of the Testis: Control Group. D: H&E-Stained Histological Assay of the Testis: Tumor Cells Not Observed in Tubules and Interstitial Spaces.

*: Significance difference in viability within each group (P≤0.05)

et al., faced challenges with FACS and MACS in germ cell isolation, leading to tumor recurrence [12]. Dovey et al., achieved high purity in separating human SCs from tumor cells using FACS, resulting in no tumor development post-transplantation [14]. Other research has explored the use of cisplatin-loaded PLGA NPs to eradicate cancerous cells from SCs [15,16]. In our study, we investigated the potential of gold NPs in purging malignant cells from the SC population. The nanoparticles employed had dimensions of 20.43 ± 2.18 nm in length, 5.55 ± 1.56 nm in width, and 2.56 ± 0.62 nm in thickness, with a folate-modified silica coating. Survival analysis revealed survival rates of 49 ± 3% for SCs and 12.33 ± 2.51% for cancer cells. Apoptosis rates post-exposure to gold nanoparticles were significantly higher in tumor cells compared to SCs (32.9 ± 2.58% vs. 51.06 ± 5.9%) [6]. Nanotechnology offers promising avenues in cancer therapy, particularly through hyperthermia treatments where temperatures range

from 41 to 48°C [17]. By harnessing laser energy in nanotherapy, specific cell populations can be targeted without harming neighboring cells [8]. Nanoparticles, owing to their small size, biocompatibility, and ability to absorb external energy, facilitate localized and systemic heating of tumor cells [18]. Various studies have explored the application of lasers with different powers in photothermal therapy. Wu et al. utilized polydopamine-coated polyester particles on HeLa and HepG2 cells, subjecting them to NIR laser irradiation for 10 minutes at 2 W, yielding promising results [19]. Similarly, Manivasagan et al. investigated the efficacy of chitosan-polypyrene-based nanocomposites on MDA-MB-231 cells, exposing them to an 808 nm laser at 2.0 W for 5 minutes, leading to notable cell death [20]. Notably, gold nanorods (GNRs) stand out among various nanoparticle types due to their superior ability to convert light into heat by absorbing NIR radiation [21].

In this study, we investigated the comparative efficacy of F-Si-GNRs and laser therapy in isolating SCs from tumor cells. Our experimental protocol involved a 6-hour incubation of both normal and cancerous cells with an optimal dose of 100 µM F-Si-GNRs, followed by a 5-minute irradiation with a 2.5 W laser, before assessing cell viability and apoptosis. Notably, we observed a significant discrepancy in the viability of healthy versus cancer cells during this process, aligning with outcomes from analogous photothermal treatment investigations [22]. Unlike findings from our previous study [6], the viability of EL4 cells and SCs did not exhibit substantial alterations. We also examined temperature fluctuations subsequent to laser exposure, with and without the presence of nanoparticles. Laser irradiation caused the temperature of healthy cells to rise to 34.2°C, escalating to 39.5°C after 6 hours of NP incubation and laser treatment. Conversely, cancer cells experienced a temperature increase to 40.1°C post-irradiation, surging to 56.2°C after photothermal therapy. In the co-culture scenario, healthy and cancer cell temperatures elevated to 36.6°C and 43.4°C, respectively. Consequently, our findings suggest that the thermal impact of the laser is contingent upon the presence of gold nanoparticles in the culture medium, corroborating observations by Yang et al. [23]. It has been established that tumor cells typically exhibit a lower pH compared to healthy cells, rendering them more susceptible to thermal stress and prone to premature cell death [23]. In line with this, Mackey et al., investigated the impact of gold nanorod size on photothermal therapy efficacy using oral epithelial carcinoma cells (HSC-3). They tested gold nanorods of varying dimensions (38 × 11 nm, 28 × 8 nm, and 5 × 17 nm) alongside an 808 nm, 5.8 W laser. Remarkably, they found that gold nanorods measuring 28 × 8 nm demonstrated enhanced cytotoxicity, highlighting the significance of nanorod size in maximizing electromagnetic field and particle transport, consistent with our own findings [24]. Yang et al., conducted a study where gold nanorods conjugated with EGFR antibody were injected into bladder tumor cells, subsequently irradiated with an 808 nm, 2.1 W laser. Their findings indicated that while laser treatment alone had negligible effects on tumor volume, nanoparticle injection resulted in a notable reduction in tumor size [23]. Similarly, Mendes et al. incubated PEG-coated rod nanoparticles in breast cancer cells before subjecting them to a 520 nm, 3.4 W laser for 60 seconds. They observed temperature increases approaching 40°C and 52°C in the laser-only and laser-nanoparticle incubation groups, respectively [25]. Interestingly, Mendes et al., reported that laser treatment alone did not induce cellular destruction, contrasting with our own observations in the laser-exposed group, where cancer cell temperatures increased by 16 degrees. This discrepancy underscores the diverse outcomes observed across different experimental setups [26]. Notably, our findings diverge significantly from those of Mohan et al., who observed a mere 2 °C temperature rise when cells were incubated with PEG-coated nanoparticles for 45 minutes before being irradiated for 10 minutes with an 808 nm, 2 W laser [27]. This disparity highlights the nuanced interplay between nanoparticle characteristics, laser parameters, and cellular responses in photothermal therapy.

It can be inferred that, alongside particle size, the duration of nanoparticle incubation significantly impacts toxicity. Moreover, silica coating, induced by laser overlap, triggers hyperthermia, leading to apoptosis or necrosis in cells [28]. Huang's investigation on human prostatic cancer cells PC-3 utilizing silica-coated gold nanoparticles with an 808 nm laser demonstrated a notable temperature increase [29]. Similarly, when MCF-7 cells were incubated with silica-coated gold nanoparticles and exposed to an 808 nm laser, a temperature rise was observed, closely aligning with our findings [30], Apoptosis analysis post-laser irradiation of nanoparticle-incubated cells revealed necrosis rates of 52.9 ± 1.5% in SCs and 60.9 ± 3% in EL4 cells, with corresponding viability rates of 32.9 ± 0.8% and 26.5 ± 2.2%. Notably, significant shifts in cell viability occurred pre-laser exposure, though in certain experiments, apoptosis alone ensued post-irradiation, indicating varying heat tolerance among different cell types [31].

Electron microscopy images post-laser exposure depicted cell necrosis characterized by general swelling and rapid plasma membrane integrity loss, with tumor cells exhibiting a higher necrosis rate, mirroring Wang et

al.'s findings [32]. Co-culture findings of SCs and EL4 cells post-laser treatment exhibited reduced cell counts to 30.6 ± 7.7% and 0.53 ± 0.15%, respectively. Although tumor cells weren't entirely eradicated, they failed to induce tumors post-transplantation, akin to Shabani et al.'s study, where cisplatin-loaded PLGA nanoparticles reduced EL4 cells to 0.8 ± 0.14%, preventing tumor formation upon transplantation into azoospermia mice [15].

## CONCLUSION

Our study illuminates a promising avenue in the realm of cancer therapy and regenerative medicine. By harnessing the synergistic potential of F-Si-GNRs and laser therapy, we have demonstrated an effective strategy for selectively targeting tumor cells while preserving the viability of SCs. Through a comprehensive series of experiments, we have elucidated the intricate mechanisms underlying cell death induced by photothermal therapy. Our findings underscore the importance of nanoparticle characteristics, such as size and surface modification, in dictating therapeutic efficacy. Moreover, electron microscopy imaging has provided valuable insights into the morphological changes associated with cell necrosis, further validating the effectiveness of our approach. Notably, our co-culture experiments have practical implications, showing a reduction in tumor cell count following laser treatment. This suggests a potential avenue for mitigating the risk of tumor formation post-SC transplantation, thereby offering hope for preserving fertility in pediatric cancer patients.

## ACKNOWLEDGMENTS

A grant from the Iran University of Medical Sciences (IUMS) covered the costs of this research (Number: 94-01-117-25884). The writers declare that they have no conflicting interests.

## REFERENCES

1. Hudson MM. Reproductive outcomes for survivors of childhood cancer. Obstet Gynecol. 2010; 116: 1171-1183.
2. Kaatsch P. Epidemiology of childhood cancer. Cancer Treat Rev. 2010; 36: 277-285.
3. Jahnukainen K, Hou M, Petersen C, Setchell B, Söder O. Intratesticular transplantation of testicular cells from leukemic rats causes transmission of leukemia. Cancer Res. 2001; 61: 706-710.
4. Hou M, Andersson M, Zheng C, Sundblad A, Söder O, Jahnukainen KJIjoa. Immunomagnetic separation of normal rat testicular cells from Roser's T-cell leukaemia cells is ineffective. 2009; 32: 66-73.
5. Eslahi N, Shakeri-Zadeh A, Ashtari K, Pirhajati-Mahabadi V, Tohidi Moghadam T, Shabani R, et al. In Vitro Cytotoxicity of Folate-Silica-Gold Nanorods on Mouse Acute Lymphoblastic Leukemia and Spermatogonial Cells. Cell J. 2019; 21:14-26.
6. Eslahi N, Shakeri-Zadeh A, Ashtari K, Pirhajati-Mahabadi V, Tohidi Moghadam T, Shabani R, et al. In Vitro Cytotoxicity of Folate-Silica-Gold Nanorods on Mouse Acute Lymphoblastic Leukemia and Spermatogonial Cells. Cell J. 2019; 21: 14-26.
7. Hirsch LR, Stafford RJ, Bankson JA, Sershen SR, Rivera B, Price RE, et al. Nanoshell-mediated near-infrared thermal therapy of tumors under magnetic resonance guidance. Proc Natl Acad Sci U S A. 2003; 100: 13549-13554.
8. Pitsillides CM, Joe EK, Wei X, Anderson RR, Lin CP. Selective cell targeting with light-absorbing microparticles and nanoparticles. Biophys J. 2003; 84: 4023-4032.
9. Zharov V, Letfullin R, Galitovskaya E. Microbubbles-overlapping mode for laser killing of cancer cells with absorbing nanoparticle clusters. J Physics D: Applied Physics. 2005; 38: 2571.
10. Huang YF, Sefah K, Bamrungsap S, Chang HT, Tan W. Selective photothermal therapy for mixed cancer cells using aptamer-conjugated nanorods. Langmuir. 2008; 24: 11860-11865.
11. Fujita K, Tsujimura A. Fertility preservation for boys with cancer. Reproductive medicine and biology. 2010; 9: 179-184.
12. Geens M, Van de Velde H, De Block G, Goossens E, Van Steirteghem A, Tournaye H. The efficiency of magnetic-activated cell sorting and fluorescence-activated cell sorting in the decontamination of testicular cell suspensions in cancer patients. Hum Reprod. 2007; 22: 733-742.
13. Fujita K, Tsujimura A, Miyagawa Y, Kiuchi H, Matsuoka Y, Takao T, et al. Isolation of germ cells from leukemia and lymphoma cells in a human in vitro model: potential clinical application for restoring human fertility after anticancer therapy. Cancer Res. 2006; 66: 11166-11171.
14. Dovey SL, Valli H, Hermann BP, Sukhwani M, Donohue J, Castro CA, et al. Eliminating malignant contamination from therapeutic human spermatogonial stem cells. The J Clin Investigation. 2013; 123: 1833-1843.
15. Shabani R, Ashjari M, Ashtari K, Izadyar F, Behnam B, Khoei S, et al. Elimination of mouse tumor cells from neonate spermatogonial cells utilizing cisplatin-entrapped folic acid-conjugated poly(lactic-co-glycolic acid) nanoparticles in vitro. Int J Nanomedicine. 2018; 13: 2943-2954.
16. Shams A, Shabani R, Asgari H, Karimi M, Najafi M, Asghari-Jafarabadi M, et al. In vitro elimination of EL4 cancer cells from spermatogonia stem cells by miRNA-143- and 206-loaded folic acid-conjugated PLGA nanoparticles. Nanomedicine (Lond). 2022; 17: 531-545.
17. añobre-López M, Teijeiro A, Rivas J. Magnetic nanoparticle-based hyperthermia for cancer treatment. Rep Pract Oncol Radiother. 2013; 18: 397-400.
18. Fekrazad R, Naghdi N, Nokhbatolfoghahaei H, Bagheri H. The Combination of Laser Therapy and Metal Nanoparticles in Cancer Treatment Originated From Epithelial Tissues: A Literature Review. J Lasers Med Sci. 2016; 7: 62-75.
19. Wu M, Zhang D, Zeng Y, Wu L, Liu X, Liu J. Nanocluster of superparamagnetic iron oxide nanoparticles coated with poly (dopamine) for magnetic field-targeting, highly sensitive MRI and photothermal cancer therapy. Nanotechnology. 2015; 26:115102.
20. Manivasagan P, Quang Bui N, Bharathiraja S, Santha Moorthy M, Oh YO, Song K, et al. Multifunctional biocompatible chitosan-polypyrrole nanocomposites as novel agents for photoacoustic imaging-guided photothermal ablation of cancer. Sci Rep. 2017; 7: 43593.
21. Bagley AF, Hill S, Rogers GS, Bhatia SN. Plasmonic photothermal heating of intraperitoneal tumors through the use of an implanted near-infrared source. ACS Nano. 2013; 7: 8089-8097.

22. Mehdizadeh A, Pandesh S, Shakeri-Zadeh A, Kamrava SK, Habib-Agahi M, Farhadi M, et al. The effects of folate-conjugated gold nanorods in combination with plasmonic photothermal therapy on mouth epidermal carcinoma cells. Lasers Med Sci. 2014; 29: 939-948.

23. 23.Yang X, Su LJ, La Rosa FG, Smith EE, Schlaepfer IR, Cho SK, et al. The antineoplastic activity of photothermal ablative therapy with targeted gold nanorods in an orthotopic urinary bladder cancer model. Bladder cancer. 2017; 3: 201-210.

24. Mackey MA, Ali MR, Austin LA, Near RD, El-Sayed MA. The most effective gold nanorod size for plasmonic photothermal therapy: theory and in vitro experiments. J Phys Chem B. 2014; 118: 1319-1326.

25. Mendes R, Pedrosa P, Lima JC, Fernandes AR, Baptista PV. Photothermal enhancement of chemotherapy in breast cancer by visible irradiation of Gold Nanoparticles. Sci Rep. 2017; 7: 10872.

26. Zhao Q, Wang L, Cheng R, Mao L, Arnold RD, Howerth EW, et al. Magnetic nanoparticle-based hyperthermia for head & neck cancer in mouse models. Theranostics. 2012; 2: 113-121.

27. Singh M, Harris-Birtill DC, Zhou Y, Gallina ME, Cass AE, Hanna GB, et al. Singh M, Harris-Birtill DC, Zhou Y, Gallina ME, Cass AE, Hanna GB, Elson DS. Application of Gold Nanorods for Photothermal Therapy in Ex Vivo Human Oesophagogastric Adenocarcinoma. J Biomed Nanotechnol. 2016; 12: 481-490.

28. Mallick S, Sun I-C, Kim K, Yi DK. Silica coated gold nanorods for imaging and photo-thermal therapy of cancer cells. J Nanosci Nanotechnol. 2013; 13: 3223-3229.

29. Huang HC, Rege K, Heys JJ. Spatiotemporal temperature distribution and cancer cell death in response to extracellular hyperthermia induced by gold nanorods. ACS Nano. 2010; 4: 2892-2900.

30. Huang X, El-Sayed IH, Qian W, El-Sayed MA. Cancer cell imaging and photothermal therapy in the near-infrared region by using gold nanorods. J Am Chem Soc. 2006; 128: 2115-2120.

31. 31 .Mehdizadeh A, Pandesh S, Shakeri-Zadeh A, Kamrava SK, Habib-Agahi M, Farhadi M, et al. The effects of folate-conjugated gold nanorods in combination with plasmonic photothermal therapy on mouth epidermal carcinoma cells. Lasers Med Sci. 2014; 29: 939-948.

32. Wang S, Huang P, Nie L, Xing R, Liu D, Wang Z, et al. Single continuous wave laser induced photodynamic/plasmonic photothermal therapy using photosensitizer-functionalized gold nanostars. Adv Mater. 2013; 25: 3055-3061.